Methane molecule confined in the small and large cages of structure I clathrate hydrate: Quantum six-dimensional calculations of the coupled translation-rotation eigenstates

ARTICLE *in* THE JOURNAL OF CHEMICAL PHYSICS · DECEMBER 2009

Impact Factor: 2.95 · DOI: 10.1063/1.3268623 · Source: PubMed

5 AUTHORS, INCLUDING:

Ivana Matanović
University of New Mexico
30 PUBLICATIONS **238** CITATIONS

Methane molecule confined in the small and large cages of structure I clathrate hydrate: Quantum six-dimensional calculations of the coupled translation-rotation eigenstates

Ivana Matanović,[1,2,a)] Minzhong Xu,[2] Jules W. Moskowitz,[2] Juergen Eckert,[3] and Zlatko Bačić[2,b)]
[1]*Department of Physical Chemistry, Rudjer Bošković Institute, Bijenička 54, Zagreb 10000, Croatia*
[2]*Department of Chemistry, New York University, New York, New York 10003, USA*
[3]*Materials Research Laboratory, University of California, Santa Barbara, California 93106, USA*

(Received 19 October 2009; accepted 6 November 2009; published online 9 December 2009)

We report fully coupled quantum six-dimensional (6D) calculations of the translation-rotation (T-R) energy levels of CH_4 molecule inside the small dodecahedral (5^{12}) and large tetracaidecahedral ($5^{12}6^2$) cages of the structure I clathrate hydrate. The quantum dynamics of the three translational and three rotational degrees of freedom of CH_4 are treated rigorously, while the guest molecule and the host cavities are taken to be rigid. The matrix of the full 6D T-R Hamiltonian is diagonalized in the product basis of contracted translational and angular basis functions, generated by solving two reduced-dimension (3D) eigenvalue problems. A pairwise additive CH_4-cage 6D potential energy surface (PES) is employed, constructed using the anisotropic CH_4—H_2O pair potential which was utilized previously in the molecular dynamics simulations of methane hydrate. Our calculations elucidate the key features of the T-R energy level structure of the nanoconfined CH_4. The rotational levels of methane exhibit an elaborate pattern of splittings caused by the angular anisotropy of the environment; the splitting patterns are identical for both types of cages. Translationally excited T-R states in the small cage are assigned in terms of the quantum numbers n and l of the 3D isotropic harmonic oscillator and those in the large cage using the Cartesian quantum numbers. Extensive comparison is made with the data from the inelastic neutron scattering studies of methane hydrate, allowing an assessment of the accuracy of the 6D PES employed. © *2009 American Institute of Physics*. [doi:10.1063/1.3268623]

I. INTRODUCTION

Clathrate hydrates are crystalline inclusion compounds where a variety of small molecules is encapsulated inside closely packed polyhedral cavities within the host lattice formed by hydrogen-bonded water molecules.[1–3] The most abundant natural form of clathrate hydrate is methane hydrate, whose vast deposits exist in deep-sea sediments and the permafrost.[4,5] The interest in methane hydrate is driven in part by the possibility that they could be a major energy resource in the future, as well as by the speculations about the role that it may have played in past climate changes and the possibility that it could do so again. Even by conservative current estimates, methane hydrate is the largest source of hydrocarbon on Earth; the amount of energy in the hydrate may very well be twice that of all other fossil fuels combined.[4,5] However, methane is also a potent greenhouse gas, and there are concerns about the impact that a large uncontrolled release of methane due to the destabilization of the ocean hydrates might have on the global climate.[4,5] Achieving quantitative understanding of methane hydrates on both microscopic and macroscopic levels is essential for reliable assessment of the feasibility of the utilization of their deposits as a source of fuel, and the risks of sudden release of methane as a result of the large-scale exploitation of the hydrates.

Methane hydrate crystallizes in the cubic structure known as the structure type I (sI). The unit cell contains 46 water molecules arranged in the hydrogen-bonded framework comprised of eight cages which fall into two types: (i) six tetracaidecahedral, or large cages which have an ellipsoidal shape, with 12 pentagonal and 2 hexagonal faces ($5^{12}6^2$) formed by 24 water molecules, and (ii) two pentagonal dodecahedra, or small, nearly spherical cages having 12 pentagonal faces (5^{12}) formed by 20 water molecules.[1,6,7] Each cage, large and small, is occupied by one CH_4 molecule, resulting in the nominal stoichiometry $CH_4 \cdot 5.75\ H_2O$.

Confining a molecule inside a nanoscale cavity leads to the quantization of the three translational degrees of freedom of its center of mass (cm), in addition to its quantized rotational states. This opens the door for the investigations of the dynamics of coupled translational and rotational motions of the guest molecule, and how it is affected by the size, shape, symmetry, and chemical composition of the host cavity, as well as the identity of the trapped molecule. When the guest is H_2, the molecule with the smallest mass and the largest rotational constant, the discrete translational and rotational states are energetically well separated. The sparse translation-rotation (T-R) energy level structure and the zero-

a)Electronic mail: imatanov@irb.hr.
b)Electronic mail: zlatko.bacic@nyu.edu.

point energy (ZPE) of the coupled T-R motions, which is substantial relative to the well depth of the interaction potential, make the dynamics of the nanoconfined hydrogen molecule highly quantum mechanical, especially at the low temperatures at which most of the experiments on them are performed. In the past couple of years, in a series of papers, we investigated rigorously for the first time the quantum dynamics of hydrogen molecules trapped in the small[8,9] and large cages[10,11] of the structure II clathrate hydrates. These studies quantified the T-R energy level structure and elucidated the quantum numbers appropriate for assigning the translational excitations and their connection with the cage symmetry, and the distinctive splitting patterns of the rotational excitations. Recently, we extended our quantum dynamics calculations to H_2 encapsulated in the fullerenes C_{60} (Refs. 12–14) and C_{70} (Ref. 14). They revealed strong coupling between the orbital angular momentum of the cm of H_2 and the rotational angular momentum of the molecule, giving rise to distinctive degeneracy patterns which differ qualitatively for the nearly isotropic C_{60} and the more anisotropic C_{70}.

CH_4 is considerably heavier than H_2 and therefore its translational dynamics in nanocages can be expected to be somewhat more classical, less dominated by quantum effects, than that of the nanoconfined H_2. However, the rotational constant of CH_4, $B_{CH_4}=5.241$ cm^{-1} (Ref. 15), is sufficiently large relative to the rather weak anisotropy of the guest-host interaction for the molecule to behave as a quantum rotor. Transitions between the three lowest rotational states of CH_4 have been measured by the inelastic neutron scattering (INS) spectroscopy at the excitation energies from 8 to 27 cm^{-1} (Refs. 16–19), as well as the $0\rightarrow 1$ rotational transition of CD_4 at 3.2 cm^{-1} (Ref. 20). Quantitative description of the excitations involving the quantum rotor states of the encapsulated CH_4/CD_4 and their coupling to the translational motions of the molecules cannot be achieved by the classical molecular dynamics (MD) simulations, and requires a quantum dynamics calculation of the fully coupled T-R eigenstates of the methane molecule inside the clathrate hydrate cages.

The dynamics of methane hydrate for excitations below ~ 30 cm^{-1} is dominated by the low-lying CH_4 quantum rotor transitions.[19] At slightly higher energies, the INS spectrum of $CH_4—D_2O$ hydrate at $T=150$ K shows a broad but distinct peak at ~ 40 cm^{-1} and a broad shoulder in the region 55–100 cm^{-1} (Refs. 21 and 22); the water lattice was deuterated in order to suppress the contribution of the host lattice phonons to the spectrum. These excitations were fitted with three Gaussians, giving peaks at 43.6, 61.3, and 80.7 cm^{-1} (Ref. 21). The two-lower frequency peaks have been assigned to the translational excitations of CH_4 along the long and short axes of the (slightly oblate) ellipsoidal large cage, respectively, while the highest-frequency peak has been attributed to the CH_4 translational fundamental in the more isotropic small cage.[21] However, unambiguous assignment of the two shoulder peaks is complicated by the contributions of the host lattice vibrations in the same energy range. The INS difference spectrum of $CH_4—H_2O$ and $CH_4—D_2O$ hydrates and the INS spectrum of $CD_4—H_2O$ hydrate at $T=100$ K, both taken with the aim to minimize the contribution of the methane molecule to the INS spectra, have maxima around 56–59 and 85–89 cm^{-1}, attributed to the (transverse acoustic) water framework modes.[21] In addition, the INS spectrum of $CD_4—H_2O$ hydrate at $T=100$ K exhibits a peak at 39.1 cm^{-1}, which has been interpreted to arise primarily from the vibration of CD_4 along the long axes of the large cage but mixed with the host lattice modes.[21]

To date, the properties of methane hydrate have been investigated theoretically using classical MD simulations[23–31] and lattice dynamics calculations.[21,22,32] These studies provided considerable insight into the translational motions of CH_4 in the small and large clathrate cages, the vibrations of the host lattice, and the coupling between the guest and host lattice vibrational modes. Their results have been very useful for the assignment and interpretation of the INS spectra of methane hydrate. But, as pointed out earlier, the issues of the rotational excitations of the caged methane and their coupling to the guest molecule (discretized) translations lie beyond the scope of the classical simulations and have not been addressed by theory so far.

This situation motivated us to perform quantum six-dimensional (6D) calculations of the T-R dynamics of methane molecule in the small and large cages of the sI clathrate hydrate, which are reported in this paper. The approach we took is an extension of that devised by us earlier to compute the (5D) T-R eigenstates of H_2 molecule inside the cages of the sII clathrate hydrate[8–11] and fullerenes.[12–14] The clathrate cages and CH_4 are taken to be rigid, while the three translational and three rotational degrees of freedom of the confined CH_4 are treated explicitly, as anharmonic and fully coupled, without any dynamical approximations. The 6D energy levels and wave functions are obtained by diagonalizing the matrix representation of the T-R Hamiltonian in a suitable contracted basis; they are numerically exact for the 6D intermolecular potential energy surface (PES) employed.

Treating CH_4 as rigid is justified by the fact that its intramolecular vibrational frequencies are much higher than the T-R excitations considered in this work and therefore weakly coupled to them. But, both the INS spectra of CH_4 hydrate (Refs. 22) and the theoretical simulations[21,22,26,28,32] revealed considerable overlap of the frequencies of the translations of the guest molecule with those of the water framework vibrations, and the existence of coupling between the guest and host lattice modes. It has been suggested that this coupling plays a significant role in the unusual behavior of the thermal conductivity of methane hydrate, but recent MD simulations[29,31] present a more complicated picture. We do not expect the rigid-cage approximation in the case of CH_4 hydrate to be as highly accurate as it was found to be for H_2 hydrate.[8–11] Nevertheless, we believe that the well defined model of CH_4 inside a rigid clathrate cage captures realistically most of the essential features of the quantum T-R dynamics of CH_4 hydrate, and for the first time sheds light on the quantum 6D T-R energy level structure of CH_4 in the small and large cavities of the sI clathrate. Therefore, the information provided by our quantum dynamics calculations,

which is presented in this paper, is complementary to that which has emerged from the classical MD and lattice dynamics simulations.

The computational methodology described in this paper is by no means limited to methane in nanocages of a clathrate hydrate; it can be used to calculate the quantum 6D T-R eigenstates of CH_4 (or any other spherical top) which is weakly bound to a rigid substrate, or trapped inside a nanocavity (e.g., zeolite, fullerene, etc.), of an arbitrary shape provided that the 6D intermolecular PES is available. Generalization to rigid rotors of lower symmetry is straightforward.

II. THEORY

A. Quantum 6D calculation of the translation-rotation eigenstates of a nanoconfined methane molecule

The computational approach developed in the course of this work employs a set of six coordinates $\{x,y,z,\theta,\phi,\chi\}$; x, y, and z are the Cartesian coordinates of the cm of the guest polyatomic molecule (CH_4), while the three Euler angles θ, ϕ, and χ specify the orientation of the molecule within the nanocage. The coordinate system is aligned with the three principal axes of the cage, and its origin is at the cm of the cage. The cavities considered belong to the 3D crystalline framework; therefore, they are treated as infinitely heavy and nonrotating. In this case, the 6D Hamiltonian for the T-R motions of the caged spherical top (CH_4) is

$$H = -\frac{\hbar^2}{2m}\left(\frac{\partial^2}{\partial x^2}+\frac{\partial^2}{\partial y^2}+\frac{\partial^2}{\partial z^2}\right)+B\mathbf{j}^2+V(x,y,z,\theta,\phi,\chi), \tag{1}$$

where m is the mass of the guest molecule, while B and $\mathbf{j}^2$ are the rotational constant and angular momentum operator, respectively, of the spherical top. $V(x,y,z,\theta,\phi,\chi)$ in Eq. (1) is the 6D PES describing the intermolecular interaction between the guest molecule and the host cage. The methodology used to calculate the energy levels and wave functions of the 6D T-R Hamiltonian in Eq. (1) is an extension of that developed by us previously to compute the 5D intermolecular vibrational energy levels of Ar_nHF clusters,[33] and later adapted for the 5D T-R eigenstates of a hydrogen molecule inside the clathrate hydrate cages[8,11] and in fullerenes.[12,14] Since a detailed description of this method is available,[33] in this section we focus on its implementation for a spherical top molecule. The 3D direct-product potential-optimized[34,35] discrete variable representation[36] (PO-DVR) denoted $\{|X_\alpha^{\mathrm{PO}}\rangle|Y_\beta^{\mathrm{PO}}\rangle|Z_\gamma^{\mathrm{PO}}\rangle\}$ is employed for the x, y, and z coordinates, while the normalized Wigner functions $D^j_{mk}(\mathbf{\Omega})$ are used as the basis for the angular coordinates $\mathbf{\Omega}=(\theta,\phi,\chi)$. Together, they constitute the 6D direct-product basis $\{|X_\alpha^{\mathrm{PO}}\rangle|Y_\beta^{\mathrm{PO}}\rangle|Z_\gamma^{\mathrm{PO}}\rangle|jmk\rangle\}$, $|jmk\rangle$ being the normalized Wigner functions $D^j_{mk}(\mathbf{\Omega})$:

$$|jmk\rangle = \left[\frac{2j+1}{8\pi^2}\right]^{1/2} D^{j*}_{mk}(\mathbf{\Omega}) = \left[\frac{2j+1}{8\pi^2}\right]^{1/2} e^{im\phi}d^j_{mk}(\theta)e^{ik\chi}. \tag{2}$$

In this 6D basis, the indices α, β, and γ label the grid points $\{X_\alpha^{\mathrm{PO}}\}$, $\{Y_\beta^{\mathrm{PO}}\}$, and $\{Z_\gamma^{\mathrm{PO}}\}$ of the 1D PO-DVRs in x, y, and z, while j, m, and k denote the total rotational angular momentum and their projections along the molecule- and space-fixed axes, respectively. The dimensions of the 1D PO-DVRs in x, y, and z are N_x^{PO}, N_y^{PO}, and N_z^{PO}.

When calculating the matrix elements of the Hamiltonian in Eq. (1) in the 6D basis $\{|X_\alpha^{\mathrm{PO}}\rangle|Y_\beta^{\mathrm{PO}}\rangle|Z_\gamma^{\mathrm{PO}}\rangle|jmk\rangle\}$, the most time consuming step is the evaluation of the potential matrix elements $\langle j'm'k'|V(X_\alpha^{\mathrm{PO}},Y_\beta^{\mathrm{PO}},Z_\gamma^{\mathrm{PO}},\mathbf{\Omega})|jmk\rangle$ at every PO-DVR point $(X_\alpha^{\mathrm{PO}},Y_\beta^{\mathrm{PO}},Z_\gamma^{\mathrm{PO}})$. For this purpose, we chose to expand the angular dependence of the potential in terms of Wigner D-functions in Eq. (2) as

$$V(X_\alpha^{\mathrm{PO}},Y_\beta^{\mathrm{PO}},Z_\gamma^{\mathrm{PO}},\mathbf{\Omega}) = \sum_{jmk} c^j_{mk}(X_\alpha^{\mathrm{PO}},Y_\beta^{\mathrm{PO}},Z_\gamma^{\mathrm{PO}})D^j_{mk}(\mathbf{\Omega}), \tag{3}$$

with the expansion coefficients evaluated as

$$c^j_{mk}(X_\alpha^{\mathrm{PO}},Y_\beta^{\mathrm{PO}},Z_\gamma^{\mathrm{PO}}) = \frac{2j+1}{8\pi^2}\int\int\int D^{j*}_{mk}(\mathbf{\Omega})V(X_\alpha^{\mathrm{PO}},Y_\beta^{\mathrm{PO}},Z_\gamma^{\mathrm{PO}},\mathbf{\Omega})d\mathbf{\Omega}, \tag{4}$$

where the angle element $d\mathbf{\Omega}$ is $d\phi\sin\theta d\theta d\chi$. This allows us to compute the potential matrix elements analytically, since the integral over a product of three Wigner D-functions can be expressed in terms of Clebsch–Gordan coefficients,[37,38]

$$\begin{aligned}\langle j'm'k'|V(X_\alpha^{\mathrm{PO}},Y_\beta^{\mathrm{PO}},Z_\gamma^{\mathrm{PO}},\mathbf{\Omega})|jmk\rangle &= \frac{(2j'+1)^{1/2}(2j+1)^{1/2}}{8\pi^2}\sum_{j''m''k''} c^{j''}_{m''k''}(X_\alpha^{\mathrm{PO}},Y_\beta^{\mathrm{PO}},Z_\gamma^{\mathrm{PO}})\\ &\times\int D^{j'}_{m'k'}(\mathbf{\Omega})D^{j''}_{m''k''}(\mathbf{\Omega})D^{j}_{mk}(\mathbf{\Omega})d\mathbf{\Omega}\\ &= \left(\frac{2j+1}{2j'+1}\right)^{1/2}\sum_{j''m''k''} c^{j''}_{m''k''}(X_\alpha^{\mathrm{PO}},Y_\beta^{\mathrm{PO}},Z_\gamma^{\mathrm{PO}})\langle jk,j''k''|j'k'\rangle\\ &\times\langle jm,j''m''|j'm'\rangle.\end{aligned} \tag{5}$$

The 3D numerical integration in Eq. (4) is performed using the Gauss–Legendre quadrature in θ and the Gauss–Chebyshev quadrature in ϕ and χ.

The 6D direct-product basis $\{|X_\alpha^{\mathrm{PO}}\rangle|Y_\beta^{\mathrm{PO}}\rangle|Z_\gamma^{\mathrm{PO}}\rangle|jmk\rangle\}$ would be prohibitively large for the problem at hand and has to be contracted in order to make direct diagonalization of the full Hamiltonian matrix feasible. One effective method for generating contracted basis functions, which is well suited for the 6D T-R Hamiltonian in Eq. (1), involves the diagonalization of matrices of the reduced-dimension Hamiltonians obtained from the full Hamiltonian operator by fixing certain coordinates at some reference values[39] or averaging over them.

In the present work, the first of the two such reduced-dimension (3D) Hamiltonians which we define is

$$ {}^{3D}h^{xyz} = -\frac{\hbar^2}{2m}\left(\frac{\partial^2}{\partial x^2}+\frac{\partial^2}{\partial y^2}+\frac{\partial^2}{\partial z^2}\right)+\bar{V}(x,y,z), \tag{6} $$

where $\bar{V}(x,y,z)$ is the full 6D PES in Eq. (1) averaged over the angular coordinates,

$$ \bar{V}(x,y,z) = \frac{1}{8\pi^2}\int V(x,y,z,\mathbf{\Omega})d\mathbf{\Omega}. \tag{7} $$

The 3D Hamiltonian ${}^{3D}h^{xyz}$ in Eq. (6) describes the coupled purely translational motions of the caged methane molecule treated as a spherical particle. The eigenvalues and eigenvectors of ${}^{3D}h^{xyz}$ are obtained by its diagonalization in the $\{|X_\alpha^{PO}\rangle|Y_\beta^{PO}\rangle|Z_\gamma^{PO}\rangle\}$ basis,

$$ {}^{3D}h^{xyz}|\Phi_t^{xyz}\rangle = {}^{3D}\epsilon_t^{xyz}|\Phi_t^{xyz}\rangle, \tag{8} $$

where

$$ |\Phi_t^{xyz}\rangle = \sum_{q=1}^{N_{xyz}^{PO}} {}^{3D}C_{q,t}^{xyz}|X_\alpha^{PO}\rangle|Y_\beta^{PO}\rangle|Z_\gamma^{PO}\rangle, \tag{9} $$

and $N_{xyz}^{PO}=N_x^{PO}\times N_y^{PO}\times N_z^{PO}$. The number of eigenvectors $|\Phi_t^{xyz}\rangle$ which is kept in the final basis, denoted n_t^{xyz}, is much smaller than N_{xyz}^{PO}, the dimension of the $\{|X_\alpha^{PO}\rangle|Y_\beta^{PO}\rangle|Z_\gamma^{PO}\rangle\}$ basis. This is possible because the 3D eigenvectors $\{|\Phi_t^{xyz}\rangle\}$ already contain a significant portion of the solution of the full 6D problem, and are also well adapted to the features of the PES.

The second 3D Hamiltonian,

$$ {}^{3D}h^{\theta\phi\chi} = B\mathbf{j}^2 + V(0,0,0,\theta,\phi,\chi), \tag{10} $$

is purely rotational, i.e., it describes the (hindered) rotation of the methane molecule whose cm is fixed at the cm of the cage. Its eigenvalues and eigenvectors are computed by the diagonalization in the angular basis of Wigner D-functions in Eq. (2),

$$ {}^{3D}h^{\theta\phi\chi}|\Phi_r^{\theta\phi\chi}\rangle = {}^{3D}\epsilon_r^{\theta\phi\chi}|\Phi_r^{\theta\phi\chi}\rangle, \tag{11} $$

where

$$ |\Phi_r^{\theta\phi\chi}\rangle = \sum_{w=1}^{N_{\theta\phi\chi}} {}^{3D}C_{w,r}^{\theta\phi\chi}|jmk\rangle, \tag{12} $$

and $N_{\theta\phi\chi}=(j_{max}+1)[4(j_{max}+1)^2-1]/3$. Only the first $n_r^{\theta\phi\chi}$ eigenvectors $|\Phi_r^{\theta\phi\chi}\rangle$ $(n_r^{\theta\phi\chi}<N_{\theta\phi\chi})$ are retained in the final basis, as its angular component. Together with the translational eigenvectors $\{|\Phi_t^{xyz}\rangle\}$, they form the product contracted 6D basis $\{|\Phi_t^{xyz}\rangle|\Phi_r^{\theta\phi\chi}\rangle\}$, the final basis for the full 6D T-R Hamiltonian in Eq. (1). The dimension of this basis is $n_t^{xyz}\times n_r^{\theta\phi\chi}$. The convergence of the 6D T-R eigenvalues with respect to both n_t^{xyz} and $n_r^{\theta\phi\chi}$ needs to be checked carefully.

The computational strategy above, where both the translational and the angular bases are contracted by solving the two 3D eigenvalue problems in Eqs. (8) and (11), respectively, is optimal for systems in which the guest-host interaction potential exhibits strong angular anisotropy. In that case the 3D hindered rotor eigenvectors $\{|\Phi_r^{\theta\phi\chi}\rangle\}$ provide a more compact angular basis than Wigner D-functions, hence $n_r^{\theta\phi\chi}$ is much smaller than $N_{\theta\phi\chi}$. The resulting large decrease in the size of the final 6D Hamiltonian matrix justifies the extra computational effort involved in generating the contracted angular basis and evaluating the Hamiltonian matrix elements in it.

For CH_4 hydrate, the angular anisotropy of the intermolecular PES is quite weak, and preliminary calculations showed that the size of the contracted angular basis required to achieve the desired high level of convergence was virtually equal to that of the (primitive) angular basis of Wigner D-functions in Eq. (2), i.e., $n_r^{\theta\phi\chi}\approx N_{\theta\phi\chi}$. Consequently, the calculations reported here employ the partially contracted product basis $\{|\Phi_t^{xyz}\rangle|jmk\rangle\}$, where $|\Phi_t^{xyz}\rangle$ are the 3D translational eigenvectors and $|jmk\rangle$ are the Wigner D-functions. In this basis, the matrix elements of the full 6D T-R Hamiltonian in Eq. (1) are found to be

$$ \begin{aligned} H_{tjmk}^{t'j'm'k'} &= \delta_{tt'}\delta_{j'j}\delta_{m'm}\delta_{k'k}\,{}^{3D}\epsilon_t^{xyz} - \delta_{j'j}\delta_{m'm}\delta_{k'k} \\ &\times\sum_{q=1}^{N_{xyz}^{PO}} {}^{3D}C_{q,t'}^{xyz}\bar{V}(X_\alpha^{PO},Y_\beta^{PO},Z_\gamma^{PO})\,{}^{3D}C_{q,t}^{xyz} \\ &+ \delta_{tt'}\delta_{j'j}\delta_{m'm}\delta_{k'k}Bj(j+1)\hbar^2 \\ &+ \sum_{q=1}^{N_{xyz}^{PO}} {}^{3D}C_{q,t'}^{xyz}\,{}^{3D}C_{q,t}^{xyz}\langle j'm'k'|V(X_\alpha^{PO},Y_\beta^{PO},Z_\gamma^{PO},\mathbf{\Omega}) \\ &\times|jmk\rangle. \end{aligned} \tag{13} $$

The dimension of this matrix is $n_t^{xyz}\times(j_{max}+1)[4(j_{max}+1)^2-1]/3$, which is much smaller than $N_x^{PO}\times N_y^{PO}\times N_z^{PO}\times(j_{max}+1)[4(j_{max}+1)^2-1]/3$, the size of the (primitive) 6D direct-product basis $\{|X_\alpha^{PO}\rangle|Y_\beta^{PO}\rangle|Z_\gamma^{PO}\rangle|jmk\rangle\}$.

B. Geometry of the cages

The geometries of the small (5^{12}) and large ($5^{12}6^2$) cages of sI clathrate hydrate used in the present work are shown in Fig. 1. In both cages, the oxygen atoms are placed in the positions determined by the high-resolution neutron diffraction measurements on the sI CD_4 hydrate.[6] A hydrogen atom of a framework water molecule lies on each edge of the cage, linking by a hydrogen bond the two O atoms at the corners connected by the edge. The H atoms are configurationally disordered. The calculated number of distinct hydrogen-bonding (H-B) arrangements exceeds 30 000 for the small 5^{12} cage[40] and is undoubtedly much greater for the large $5^{12}6^2$ cage. The H-B arrangements used in this work, displayed in Fig. 1, were chosen at random with the goal of distributing the nonbonded O–H bonds evenly over the exterior of the two cages.

Judging from Fig. 1, the small cage has a highly symmetric, almost spherical shape, and the large cage has the shape of an oblate ellipsoid. This impression is confirmed by the calculations of the three principal moments of inertia, and the corresponding rotational constants for the small and large cages. When only the O atoms are taken into account, all three rotational constants of the small cage turn out to be identical, 5.312×10^{-3} cm^{-1}, while for the large cage two rotational constants are the same, 3.865×10^{-3} cm^{-1}, and the third one is smaller, 3.272×10^{-3} cm^{-1} (inclusion of the water H atoms causes very small changes of these numbers).

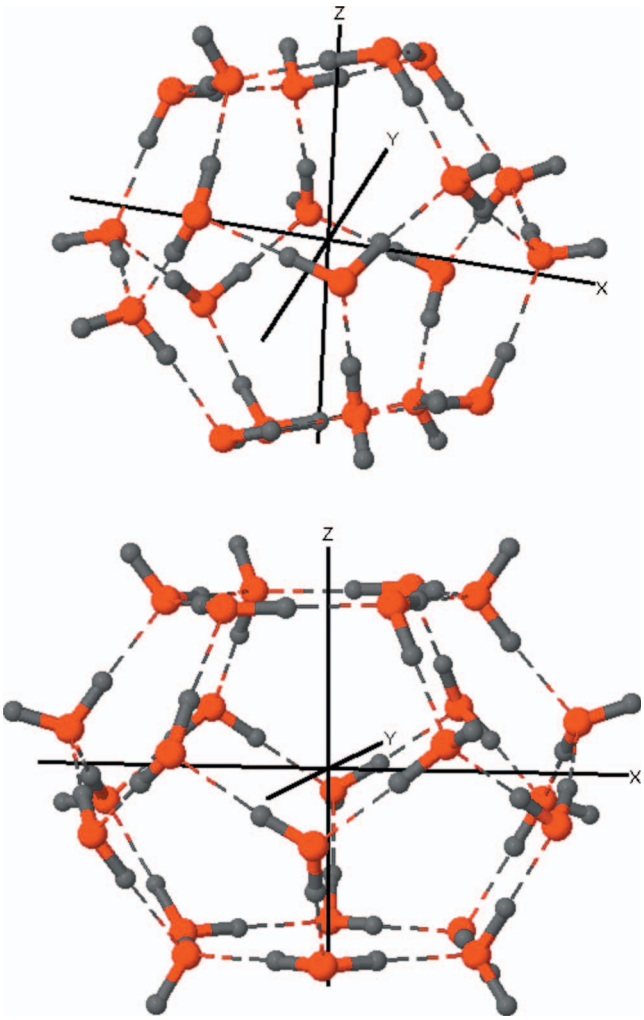

FIG. 1. Geometries of the small (5^{12}) cage (top) and the large ($5^{12}6^2$) cage (bottom) of structure I clathrate hydrate. The Cartesian axes shown coincide with the principal axes of the cages.

Hence, the small cage essentially has the symmetry of a spherical top, and the large cage has the lower symmetry of an oblate symmetric top. Therefore, the symmetry of the environment experienced by CH_4 in the small cage is higher than that of the large cage. Our recent studies of the quantum T-R dynamics of a hydrogen molecule in the small[9] and large cages[11] of sII clathrate hydrate have shown that differences of this type lead to qualitatively different T-R dynamics in the two cages, and two distinct sets of translational quantum numbers.[11]

C. Potential energy surfaces

In this initial work, the intermolecular interaction of the encapsulated methane molecule with the water nanocage is assumed to be pairwise additive, as in most classical MD simulations of CH_4 hydrate. Consequently, the interaction potential $V_{CH_4\text{-cage}}$ between the confined CH_4 and N H_2O molecules forming the cage ($N=20$ and 24 for the small and the large cage, respectively) is written as

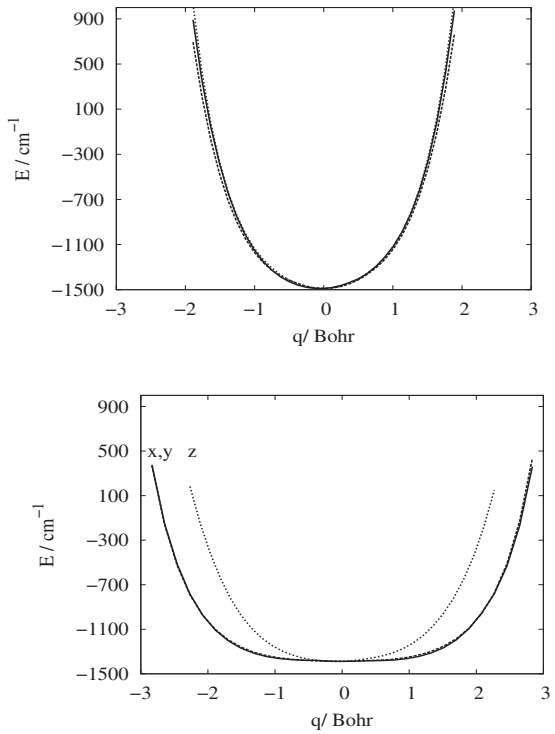

FIG. 2. One-dimensional cuts through the 6D intermolecular PESs of CH_4 in the small (top) and large cage (bottom), along the Cartesian axes $q=x,y,z$, which coincide with the principal axes of the cages. The potential profiles are obtained by minimizing the CH_4-cage interaction with respect to the three Euler angles of CH_4 at every position of its cm.

$$V_{CH_4\text{-cage}}(\mathbf{q}) = \sum_{w=1}^{N} V_{CH_4—H_2O}(\mathbf{q},\mathbf{Q}_w), \tag{14}$$

where $\mathbf{q}=(x,y,z,\mathbf{\Omega})$ are the coordinates of the methane molecule, $V_{CH_4—H_2O}$ is the pair interaction potential specified below between CH_4 and a framework H_2O molecule, and the index w runs over the water molecules of the cage, small or large, whose coordinates $\mathbf{Q}_w$ are fixed. A widely used form of the $CH_4—H_2O$ pair potential introduced by Tse *et al.*[24] combines the Coulomb interactions between the five point charges on the C and H atoms of methane and the three point charges on the H_2O molecule with the Lennard-Jones (LJ) interaction between the C atom of methane and the O atom of H_2O. It is given by

$$V_{CH_4—H_2O} = \sum_{i(CH_4)} \sum_{j(H_2O)} \frac{q_i q_j}{r_{ij}} + 4\varepsilon_{O—CH_4} \times \left[\left(\frac{\sigma_{O—CH_4}}{r_{O—CH_4}} \right)^{12} - \left(\frac{\sigma_{O—CH_4}}{r_{O—CH_4}} \right)^{6} \right], \tag{15}$$

where $r_{O—CH_4}$ is the distance between the O atom of H_2O and the C atom of CH_4. The point charges q_i, $i=1-5$, are placed on the atoms of the CH_4 molecule, positive charges of $+0.14e$ on each of its H atoms and one negative charge of $-0.56e$ on the C atom. The charges q_j, $j=1-3$, on the H_2O molecule are taken from the SPC/E effective pair potential model for water,[41] $-0.8476e$ on the O atom and $+0.4238e$ on each H atom. The second term in Eq. (15) represents the LJ interactions between the O atom of H_2O and the C atom of

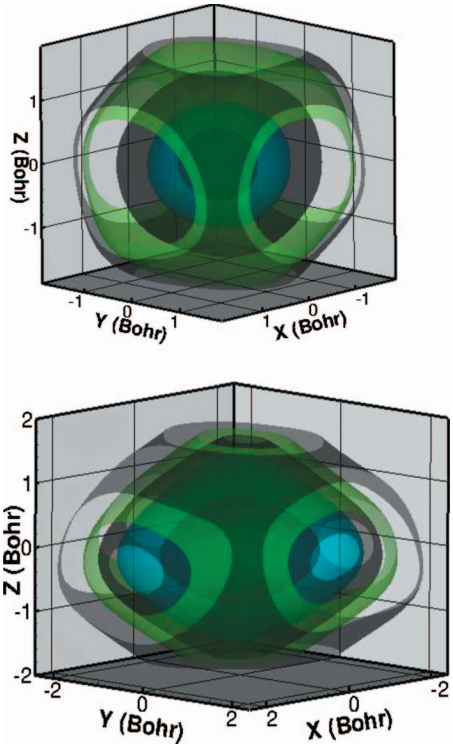

FIG. 3. Top: 3D isosurfaces at −1400, −1100, −700, 700, and 1400 cm^{-1} for the 6D intermolecular PES of CH_4 in the small cage. Bottom: 3D isosurfaces at −1300, −1000, −700, 700, and 1300 cm^{-1} for the 6D intermolecular PES of CH_4 in the large cage. The isosurfaces are obtained by minimizing the CH_4-cage interaction with respect to the three Euler angles of CH_4 at every position of its cm.

CH_4. The LJ parameters $\varepsilon_{O—CH_4}$ and $\sigma_{O—CH_4}$ are determined following the standard Lorentz–Berthelot combination rules, $\varepsilon_{ij}=(\varepsilon_{ii}\varepsilon_{jj})^{1/2}$ and $\sigma_{ij}=(\sigma_{ii}+\sigma_{jj})/2$, which give $\sigma_{O—CH_4}=6.431$ a.u. and $\varepsilon_{O—CH_4}=73.099$ cm^{-1}.

Different empirical intermolecular PESs have been used in the computer simulations of methane hydrates.[30] Most of them are pairwise additive, although some MD simulations employed polarizable force fields.[26,28] Any one of them could be implemented in our quantum 6D bound-state calculations. We chose the CH_4-water nanocage interaction potential by Tse *et al.*[24] for this study because of its simplicity and because it was used previously in several classical MD simulations of CH_4 hydrate.[16,24,26,30]

The 1D profiles of the 6D PES for CH_4 in the small and large cages defined by Eqs. (14) and (15) along each of the three Cartesian axes are shown in Fig. 2. For the small cage, the three 1D potential cuts are virtually indistinguishable, in accordance with the high symmetry of this cage (spherical top) which was discussed in Sec. II B. In contrast, for the large cage, the 1D cuts along x and y axes are identical, and different from the 1D cut along the z axis. The 1D profile along the z axis is tighter and restricts the motion of CH_4 more, than the 1D profiles in the x and y directions. This potential anisotropy is consistent with, and indeed expected from, the oblate symmetric top symmetry of the large cage discussed in Sec. II B. Figure 3 displays the 3D isosurfaces of the 6D PES for CH_4 in the small and large cages, which clearly reflect the shapes of the two cages.

D. Computational details

In the calculation reported here, the dimensions of the 1D PO DVRs in the small cage were $N_x^{PO}=N_y^{PO}=N_z^{PO}=13$, and they spanned the range $-1.89\leq\lambda\leq1.89$ a.u. $(\lambda=x,y,z)$. For the large cage, the dimensions of the 1D PO DVRs were $N_x^{PO}=N_y^{PO}=17$ and $N_z^{PO}=13$; they were distributed over the range $-2.84\leq\lambda\leq2.84$ a.u. $(\lambda=x,y)$ and $-2.27\leq z\leq2.27$ a.u. The angular basis $|jmk\rangle$ used for both cages included functions up to $j_{max}=5$, which meant using 286 Wigner D-functions. In expanding the angular dependence of the 6D PES in Eq. (3), 1771 Wigner D-functions up to $j_{max}=10$ were used. For the small cage, the lowest $n_t^{xyz}=35$ translational eigenvectors $|\Phi_t^{xyz}\rangle$ were retained in the final basis, while for the large cage n_t^{xyz} was 55. Consequently, the dimensions of the final 6D T-R Hamiltonian matrices were $35\times286=10\,010$ for the small cage, and $55\times286=15\,730$ for the large cage. They are much smaller than the dimensions these matrices would have in the primitive 6D direct product basis $\{|X_\alpha^{PO}\rangle|Y_\beta^{PO}\rangle|Z_\gamma^{PO}\rangle|jmk\rangle\}$, $13\times13\times13\times286=628\,342$ for the small cage and $17\times17\times13\times286=1\,074\,502$ for the small cage. The calculated 6D T-R excitation energies up to 200 cm^{-1} in the small cage and up to 150 cm^{-1} in the large cage are converged to five significant figures. The rotational constant of methane used in our calculation, $B_{CH_4}=5.244$ cm^{-1}, was calculated from the methane geometry with the C−H bond length of 1.094 Å. For comparison, the rotational constant of CH_4 in the ground vibrational state determined from the high resolution IR spectra[15] has the value of 5.241 cm^{-1}.

III. RESULTS AND DISCUSSION

Prior to analyzing the coupled 6D T-R energy levels of CH_4 in the small and large cages, we decided to investigate the 3D translations and the 3D rotations of the caged methane molecule separately. The objective was to gain a clear understanding of the basic features of the quantum 3D dynamics of the translations and rotations of CH_4 in the limit when they are uncoupled and unobscured by the higher density of the 6D T-R levels and complications arising from the T-R coupling. For translations, we solved the 3D eigenvalue problem defined by Eqs. (6)–(9), and for rotations the 3D eigenvalue problem defined by Eqs. (10)–(12). Having the information about the energy level structure, degeneracy patterns, and quantum number assignments for the separate translational and rotational excitations proved very valuable in the analysis of the coupled 6D T-R eigenstates and in assessing the extent of the T-R coupling. The 3D translational excitations in the small and large cages are discussed in Sec. III A, and the 3D rotational excitations are discussed in Sec. III B. The coupled 6D T-R excitations in the small and large cages are analyzed in Sec. III C, and comparison between our results and spectroscopic data is made in Sec. III D.

TABLE I. Translational energy levels of CH_4 in the small cavity of sI clathrate hydrate, from the quantum 3D calculations. The translational excitation energies ΔE^{trans} are relative to the ground-state energy $E_0^{trans} = -1337.1\ cm^{-1}$. The rms amplitudes Δx, Δy, and Δz are in bohr. The quantum numbers n and l are those of the 3D isotropic HO.

n	ΔE^{trans}	Δx	Δy	Δz	
1	0.0	0.23	0.23	0.23	$n=0,\ l=0$
2	71.5	0.35	0.23	0.29	
3	71.5	0.23	0.38	0.23	$n=1,\ l=1$
4	71.6	0.28	0.24	0.34	
5	143.7	0.41	0.32	0.27	
6	144.0	0.25	0.36	0.40	
7	145.5	0.27	0.35	0.39	$n=2,\ l=2$
8	145.5	0.38	0.33	0.30	
9	145.5	0.35	0.35	0.32	
10	147.8	0.34	0.34	0.34	$n=2,\ l=0$
11	218.9	0.32	0.46	0.35	
12	218.9	0.33	0.34	0.46	
13	218.9	0.48	0.33	0.33	
14	220.2	0.36	0.40	0.39	$n=3,\ l=3$
15	220.2	0.38	0.38	0.39	
16	220.3	0.42	0.37	0.36	
17	222.0	0.38	0.38	0.38	
18	225.1	0.45	0.33	0.32	
19	225.1	0.32	0.45	0.35	$n=3,\ l=1$
20	225.2	0.34	0.33	0.45	

TABLE II. Translational energy levels of CH_4 in the large cavity of sI clathrate hydrate, from the quantum 3D calculations. The translational excitation energies ΔE^{trans} are relative to the ground-state energy $E_0^{trans} = -1311.1\ cm^{-1}$. The rms amplitudes Δx, Δy, and Δz are in bohr. The energy levels are assigned in terms of the Cartesian quantum numbers (v_x,v_y,v_z) whenever possible, or as $[\mathcal{N}_{xy},v_z]$, where $\mathcal{N}_{xy}$ is the total number of quanta in the x and y modes. For additional explanation see the text.

n	ΔE^{trans}	Δx	Δy	Δz	
1	0.0	0.35	0.35	0.27	(0,0,0)
2	29.9	0.38	0.58	0.26	(0,1,0)
3	30.0	0.58	0.38	0.26	(1,0,0)
4	50.5	0.36	0.36	0.45	(0,0,1)
5	60.7	0.58	0.58	0.27	[2,0]
6	62.4	0.50	0.65	0.26	[2,0]
7	62.4	0.65	0.50	0.25	[2,0]
8	83.9	0.39	0.58	0.43	(0,1,1)
9	83.9	0.58	0.39	0.43	(1,0,1)
10	94.0	0.55	0.73	0.27	(1,2,0)
11	94.0	0.73	0.54	0.27	(2,1,0)
12	97.1	0.50	0.79	0.25	(0,3,0)
13	97.1	0.79	0.48	0.25	(3,0,0)
14	103.6	0.35	0.35	0.58	(0,0,2)
15	117.8	0.59	0.59	0.41	[2,1]
16	119.2	0.58	0.61	0.40	[2,1]
17	119.4	0.60	0.56	0.40	[2,1]

A. Quantum 3D results: Translational excitations in the small and large cages

The lower-lying translational energy levels of CH_4 in the small and large cages from the quantum 3D calculations are given in Tables I and II, respectively. Both tables show for each state the root mean squared (rms) amplitudes Δx, Δy, and Δz, which are a measure of the wave function delocalization in the x-, y-, and z-directions, respectively, and can be helpful in making the quantum number assignments.

Small cage. The 3D translational energy levels for the small cage are shown in Table I. The first three almost degenerate levels ($n=2-4$) at 71.5–71.6 cm^{-1} correspond to the fundamental translational excitations of the caged CH_4. While they could be assigned using the Cartesian quantum numbers (v_x,v_y,v_z), the energy levels with two and three quanta of excitation exhibit patterns which cannot be accounted for in a satisfactory manner with the Cartesian quantum number assignments. Thus, five of the six two-quanta excitations ($n=5-9$) are clumped together, from 143.7 to 145.5 cm^{-1}, while the sixth ($n=10$) stands apart at 147.8 cm^{-1}. Likewise, the ten three-quanta excitations appear in two groups, consisting of seven and three closely spaced states, respectively; the group of seven states ($n=11-17$) lies within the interval 218.9–222.0 cm^{-1}, while the other three states ($n=18-20$) are nearly degenerate, at 225.1–225.2 cm^{-1}.

These energy level patterns can be understood in terms of the physical picture where, for the purpose of assignment only, the translational modes are viewed as those of the 3D isotropic harmonic oscillator (HO). The energy levels of the 3D isotropic HO are labeled by the principal quantum number n and the orbital angular momentum quantum number l, whose allowed values are $n, n-2, \cdots 1$ or 0, for odd or even n, respectively.[42] When the possible values of m, $-l \le m \le l$, are taken into account, the degree of degeneracy of the energy levels of the isotropic 3D HO is $(1/2)(n+1)(n+2)$, e.g., 3 for $n=1$, 6 for $n=2$, and 10 for $n=3$.

In this picture, the five closely spaced two-quanta excitations ($n=5-9$) in Table I are understood to represent the $n=2,\ l=2$ quintuplet, and the sixth ($n=10$) is the single $n=2,\ l=0$ state. In the same vein, the two manifolds with seven ($n=11-17$) and three ($n=18-20$) three-quanta states are assigned as $n=3,\ l=3$ and $n=3,\ l=1$, respectively. The triply degenerate fundamental ($n=2-4$) corresponds to $n=1,\ l=1$. These quantum number assignments are given in Table I. It should be emphasized that although the model of the 3D isotropic HO and its quantum numbers is successful in correlating and assigning the T-R levels in the small cage, the translationally excited states are *not* harmonic. As Table I shows, their energies depend not only on n, as in the true 3D isotropic HO,[42] but also on l, evidence of their *anharmonicity*. Finally, the fact that neither the five $n=2,\ l=2$ levels nor the seven with $n=3,\ l=3$ (or the three $n=1,\ l=1$ levels) are exactly degenerate is, we believe, due to the positional disorder of the H atoms which slightly lowers the symmetry of the environment of the guest CH_4, and possibly also the "crystal field" of the cage, which we encountered already in our earlier studies of H_2 in large cage of sII clathrate hydrate[11] and inside C_{60}.[12,14]

The suitability of the 3D isotropic HO model for the assignment of the translational excitations of CH_4 in the small cage was anticipated in view of the essentially

spherical-top geometry of the cage (Sec. II B) and the correspondingly high symmetry of the interaction potential evident from Fig. 2 (top). The same set of translational quantum numbers was found to be appropriate in our previous investigations of H_2 confined in large cage of sII clathrate hydrate[11] and C_{60}.[12,14] Both are spherical tops, the former to a high degree and the latter exactly.

Large cage. The 3D translational energy levels of CH_4 in the large cage are given in Table II. The wave functions and the rms amplitudes Δx, Δy, and Δz of the first two nearly degenerate levels $(n=2,3)$ at 29.9–30.0 cm^{-1} show that they represent the fundamental translational excitations along the long (x and y) axes of the large cage, while the third excited state $(n=4)$ at 50.5 cm^{-1} corresponds to the fundamental excitation of the translational mode along the short (z) axis of the cage. That the frequency of the z-mode fundamental is significantly higher than that of the x- and y-mode fundamentals reflects the greater stiffness of the PES along the z axis than in the x and y directions, which is evident from the 1D potential profiles shown in Fig. 2 (bottom). The near-degeneracy of the x- and y-mode fundamentals is also readily understood from Fig. 2 (bottom), which shows virtually identical 1D potential cuts along the x and y axes.

The splitting of the translational fundamental into two components in the large cage, unlike the small cage where the translational fundamental is practically degenerate, signals right away that the quantum numbers of the 3D harmonic HO are not applicable to the translational excitations of CH_4 in the large cage. Indeed, examination of the wave functions of the excited states in the large revealed that the majority can be assigned in terms of the Cartesian quantum numbers (v_x,v_y,v_z), by counting the number of nodal planes perpendicular to the respective axes. However, assignment of this type was not possible in some cases, such as the states $n=5-7$ and $n=15-17$. The nodal patterns of these states in the xy plane are more suggestive of the 2D isotropic HO with its quantum numbers (v,l), where v denotes the number of quanta and l is the vibrational angular momentum along the z axis. Still, we were not sufficiently confident to make unambiguous assignments of these two triplets of states, and chose to label them simply by $\mathcal{N}_{xy}$, the total number of quanta in the x and y modes, and the number of quanta in the z mode, v_z.

The possibility of using the quantum numbers of the 2D isotropic HO was not surprising for us. For H_2 in the small cage of sII clathrate hydrate[9] and inside C_{70},[14] both of which also have the symmetric-top geometries, oblate and prolate, respectively, the quantum numbers (v,l) (actually $|l|$) of the 2D isotropic HO were used successfully for assigning the in-plane xy modes, together with the Cartesian quantum number v_z for the z-mode excitation.

B. Quantum 3D results: Rotational excitations in the small and large cages

The lower-lying rotational energy levels of CH_4 in the small and large cages from the quantum 3D calculations are given in Tables III and IV, respectively. For each rotational level, its degeneracy g is shown, as well as the contributions from the $j=0-3$ rotational basis functions.

In the gas phase, the rotational energy levels of CH_4 with the quantum number j have the degeneracy of $(2j+1)^2$. Hence the degeneracy of the rotational levels $j=1$, 2, and 3, is 9, 25, and 49, respectively. However, the angular aniso-

TABLE III. Rotational energy levels of CH_4 inside the small cavity of sI clathrate hydrate, from the quantum 3D calculations for the cm of CH_4 kept fixed at the cm of the cage. The rotational excitation energies ΔE^{rot} are relative to the ground-state energy $E_0^{rot}=-1442.9$ cm^{-1}, and g denotes the degeneracy of the levels. The columns labeled $j=0-3$ show the contributions of the corresponding rotational basis functions to the eigenstates.

ΔE^{rot}	g	$j=0$	$j=1$	$j=2$	$j=3$
9.7	3	0.00	**0.92**	0.06	0.01
9.9	3	0.00	**0.94**	0.04	0.02
10.0	3	0.00	**0.95**	0.02	0.03
22.4	2	0.00	0.00	**0.98**	0.00
28.5	3	0.00	0.00	**0.98**	0.02
28.9	3	0.00	0.02	**0.93**	0.04
29.6	2	0.00	0.03	**0.93**	0.03
31.4	3	0.00	0.05	**0.87**	0.07
32.5	2	0.00	0.00	**0.99**	0.00
34.1	3	0.00	0.01	**0.95**	0.04
34.6	2	0.00	0.00	**0.99**	0.00
35.3	3	0.00	0.01	**0.95**	0.03
42.3	2	0.00	0.00	**0.97**	0.00
51.6	1	0.01	0.00	0.00	**0.97**
57.4	3	0.00	0.00	0.03	**0.95**
⋮	⋮	⋮	⋮	⋮	⋮
71.5	3	0.00	0.01	0.03	**0.95**
73.3	1	0.00	0.01	0.03	**0.95**

TABLE IV. Rotational energy levels of CH_4 inside the large cavity of sI clathrate hydrate, from the quantum 3D calculations for the cm of CH_4 kept fixed at the cm of the cage. The rotational excitation energies ΔE^{rot} are relative to the ground-state energy $E_0^{rot}=-1364.1$ cm^{-1}, and g denotes the degeneracy of the levels. The columns labeled $j=0-3$ show the contributions of the corresponding rotational basis functions to the eigenstates.

ΔE^{rot}	g	$j=0$	$j=1$	$j=2$	$j=3$
9.7	3	0.00	**0.93**	0.06	0.00
9.9	3	0.00	**0.94**	0.05	0.01
10.3	3	0.00	**0.97**	0.01	0.02
25.1	2	0.00	0.00	**0.99**	0.00
27.0	2	0.00	0.00	**1.00**	0.00
29.9	3	0.00	0.00	**0.95**	0.04
30.9	3	0.00	0.01	**0.96**	0.02
31.5	3	0.00	0.02	**0.94**	0.04
31.8	2	0.00	0.00	**0.99**	0.00
32.7	3	0.00	0.02	**0.93**	0.04
34.5	3	0.00	0.05	**0.90**	0.00
35.3	2	0.00	0.00	**0.99**	0.00
42.1	2	0.00	0.00	**0.98**	0.00
58.1	1	0.00	0.00	0.00	**0.98**
58.6	3	0.00	0.00	0.01	**0.98**
⋮	⋮	⋮	⋮	⋮	⋮
69.6	3	0.00	0.01	0.03	**0.95**
71.0	3	0.00	0.01	0.03	**0.95**

tropy of the CH_4-cage PES causes partial lifting of this degeneracy, giving rise to a rather elaborate splitting pattern of the rotational multiplets, which happen to be the same in both cages. The $j=1$ level splits into three closely spaced triply degenerate levels, at 9.7–10.0 cm^{-1} in the small cage and 9.7–10.3 cm^{-1} in the large cage. Their energies are slightly below that of the $j=1$ level in the gas phase, 10.49 cm^{-1}.

The higher rotational levels of the confined CH_4 exhibit splittings which are substantially larger and more complicated. In both cages, the $j=2$ level is split into ten sublevels, five of which are triply degenerate and the other five are doubly degenerate. They are spread over 19.9 cm^{-1} in the small cage (from 22.4 to 42.3 cm^{-1}), and over 17.0 cm^{-1} in the large cage (from 25.1 to 42.1 cm^{-1}). Roughly half of the sublevels lies below, and the other half above, the energy of the $j=2$ level in the gas phase, 31.46 cm^{-1}. The $j=3$ level appears split into 21 sublevels, 7 nondegenerate and 14 triply degenerate, only some of which are shown in Tables III and IV. The sublevels are split by 21.7 cm^{-1} in the small cage and span the range 51.6–73.3 cm^{-1}; in the large cage, they are split by 12.9 cm^{-1}, over the range 58.1–71.0 cm^{-1}. As in the case of the $j=2$ level, the $j=3$ sublevels lie below and above the gas-phase energy of the $j=3$ level, 62.93 cm^{-1}. For all the rotational levels considered, j is a good quantum number, since the contribution of the dominant rotational basis function to the eigenstate is generally greater than 0.9.

Rotational level splittings of comparable magnitudes (for the $j=1$ and $j=2$ levels) were found in our previous quantum 5D calculations of H_2 in the small[8,9] and large[11] cages of sII clathrate hydrates, and also observed experimentally.[43–45]

The splitting patterns of the rotational levels in Tables III and IV undoubtedly have a group-theoretical explanation. The finding that the $j=2$ sublevels exhibit double and triple degeneracy is certainly related to the fact that the $j=2$ rotational wave functions of CH_4 (T_d symmetry) belong to the irreducible representations (IRs) e (2D) and t_2 (3D). Likewise, the splitting of the $j=3$ level into only nondegenerate and triply degenerate sublevels must have a connection with the $j=3$ wave functions belonging to the IRs a_2 (1D), t_1 (3D), and t_2 (3D). For a given j value, the number of times each IR appears is $2j+1$. A rigorous group-theoretical treatment of this problem would have to take into account both the symmetry of the guest molecule and of the host cage, using the extended group formalism,[46] which has been utilized to analyze the rovibrational states of the methane molecule in solid parahydrogen.[47,48] Such a detailed study does not belong in this exploratory methodological and computational paper, and is left for future work.

C. Quantum 6D translation-rotation energy levels in the small and large cages

The T-R energy levels from the quantum 6D calculations of CH_4 in the small and large cages are given in Tables V and VI, respectively. The density of T-R energy levels is high, especially in the large cage. The T-R levels shown in Tables V and VI, which correspond to the low-lying rotational and translational excitations, have been selected from a large number of the computed T-R states in this energy range. For each level listed, the two tables give its degeneracy g, the rms amplitudes Δx, Δy, and Δz, and the contributions from the $j=0-3$ rotational basis functions to the wave function. Shown in the last column are the assignments of the translational excitations, using the quantum numbers n and l of the 3D isotropic HO for the small cage (Table V), and the Cartesian quantum numbers (v_x,v_y,v_z) for the large cage (Table VI). These assignments were made by inspecting the changes in the rms amplitudes, as well as the 3D reduced probability densities (RPDs) $\rho_n(x,y,z)$ in the Cartesian coordinates,

$$\rho_n(x,y,z) = \int \psi_n^*(x,y,z,\mathbf{\Omega})\psi_n(x,y,z,\mathbf{\Omega})\sin\,\theta d\theta d\phi d\chi, \tag{16}$$

where $\psi_n(x,y,z,\mathbf{\Omega})$ is the 6D T-R wave function of the encapsulated CH_4. The 3D RPDs of some 6D T-R eigenstates in the large cage, which are sufficiently regular to allow the assignment of quantum numbers, are shown in Figs. 4 and 5. The excitation energies ΔE are relative to T-R ground state of the encapsulated CH_4, −1339.9 cm^{-1} in the small cage and −1313.3 cm^{-1} in the large cage. Since the global minimum of the 6D PES for the small cage is at −1505.1 and −1420.3 cm^{-1} for the large cage, the ZPE of the T-R motions is equal to 165.2 and 107.0 cm^{-1} in the small and large cages, respectively.

1. Rotational excitations

The lowest-lying 6D T-R energy levels in both cages are the rotationally excited states of CH_4 in the ground translational state. The splitting patterns of the $j=1$ and $j=2$ levels in the small and large cages given in Tables V and VI, respectively, are virtually the same and match the patterns found in the quantum 3D calculations discussed in Sec. III B; the energies of the sublevels in the two cages are very similar as well. The $j=1$ level is split into three levels, each with the threefold degeneracy, which lie in the narrow energy range of 9.6–10.0 cm^{-1} in the small cage and 9.7–10.3 cm^{-1} in the large cage. These energies are slightly below the $j=1$ level in the gas phase, 10.49 cm^{-1}, indicating only a weak hindrance of the CH_4 rotation. The $j=2$ level appears split into ten components, five triply degenerate and five doubly degenerate. These ten $j=2$ sublevels range from 22.6 to 42.3 cm^{-1} in the small cage, and from 25.1 to 41.5 cm^{-1} in the large cage. About half of the sublevels are energetically below, and the other half above, the $j=2$ level in the gas phase at 31.46 cm^{-1}. The $j=3$ level in the small cage is split into 21 sublevels, of which 7 are nondegenerate and 14 are triply degenerate (as in the quantum 3D calculations), and span the range 52.1–71.2 cm^{-1}. As in the case of the $j=2$ level, the gas-phase energy of the $j=3$ level, 62.93 cm^{-1}, falls roughly in the middle of this energy range. Identifying the 21 components of the $j=3$ level was relatively straightforward since in the small cage their energies are below that of the translational fundamental (74–76 cm^{-1}). But as discussed below, in the large cage the translational fundamentals (29 and 49 cm^{-1}) overlap energetically with the rotational excitations, making the identification of all $j=3$

TABLE V. Select T-R energy levels of CH_4 in the small cavity of sI clathrate hydrate, from the quantum 6D calculations. The T-R excitation energies ΔE are relative to the ground-state energy $E_0=-1339.9$ cm^{-1}. For the purely rotationally excited levels, those with ΔE up to 71.2 cm^{-1}, g denotes their degeneracy. The rms amplitudes Δx, Δy, and Δz are in bohr. The columns labeled $j=0-3$ show the contributions of the corresponding rotational basis functions to the eigenstates. The translational quantum numbers n and l are those of the 3D isotropic HO.

ΔE	g	Δx	Δy	Δz	$j=0$	$j=1$	$j=2$	$j=3$	
0.0	1	0.23	0.23	0.23	**0.97**	0.00	0.00	0.02	$n=0$, $l=0$
9.6	3	0.23	0.23	0.23	0.00	**0.92**	0.06	0.01	
9.8	3	0.23	0.23	0.23	0.00	**0.93**	0.04	0.02	$n=0$, $l=0$
10.0	3	0.23	0.23	0.23	0.00	**0.95**	0.02	0.03	
22.6	2	0.23	0.23	0.23	0.00	0.00	**0.98**	0.02	
28.4	3	0.23	0.23	0.23	0.00	0.02	**0.93**	0.04	
28.9	3	0.23	0.23	0.23	0.00	0.03	**0.93**	0.03	
29.2	2	0.23	0.23	0.23	0.00	0.00	**0.99**	0.00	
31.6	3	0.23	0.23	0.23	0.00	0.05	**0.87**	0.07	$n=0$, $l=0$
32.3	2	0.23	0.23	0.23	0.00	0.00	**0.99**	0.00	
33.9	3	0.23	0.23	0.23	0.00	0.02	**0.93**	0.05	
34.5	2	0.23	0.23	0.23	0.00	0.00	**0.99**	0.00	
34.9	3	0.23	0.23	0.23	0.00	0.02	**0.93**	0.04	
42.3	2	0.23	0.23	0.23	0.00	0.00	**0.97**	0.03	
52.1	1	0.23	0.23	0.23	0.04	0.00	0.00	**0.94**	
⋮	⋮	⋮	⋮	⋮	⋮	⋮	⋮	⋮	$n=0$, $l=0$
71.2	1	0.23	0.23	0.23	0.00	0.03	0.04	**0.91**	
73.9		0.32	0.23	0.26	**0.70**	0.00	0.00	0.28	
74.8		0.24	0.33	0.23	**0.68**	0.00	0.00	0.31	$n=1$, $l=1$
76.4		0.23	0.23	0.30	**0.40**	0.00	0.00	0.56	
147.9		0.41	0.28	0.26	**0.60**	0.00	0.00	0.37	
149.0		0.29	0.40	0.24	**0.56**	0.00	0.00	0.40	
149.5		0.31	0.35	0.31	**0.65**	0.00	0.00	0.33	$n=2$, $l=2$
150.0		0.36	0.27	0.33	**0.60**	0.00	0.00	0.36	
150.6		0.27	0.32	0.37	**0.61**	0.00	0.00	0.36	
151.5		0.29	0.31	0.37	**0.70**	0.00	0.00	0.28	$n=2$, $l=0$
223.3		0.46	0.35	0.27	**0.62**	0.00	0.00	0.35	
224.0		0.38	0.40	0.30	**0.59**	0.00	0.00	0.37	
224.9		0.36	0.36	0.38	**0.62**	0.00	0.00	0.34	
225.1		0.38	0.37	0.35	**0.63**	0.00	0.00	0.34	$n=3$, $l=3$
225.5		0.30	0.41	0.39	**0.62**	0.00	0.00	0.34	
226.1		0.37	0.35	0.38	**0.64**	0.00	0.00	0.33	
226.9		0.37	0.35	0.39	**0.67**	0.00	0.00	0.30	
228.6		0.38	0.38	0.35	**0.73**	0.00	0.00	0.23	
229.6		0.33	0.31	0.45	**0.73**	0.00	0.00	0.25	$n=3$, $l=1$
230.0		0.33	0.40	0.36	**0.73**	0.00	0.00	0.25	

sublevels much more difficult. For this reason, the $j=3$ rotational excitations in the large cage are not listed in Table VI. For the rotational excitations shown in Tables V and VI, j is a good quantum number since the weight of the dominant rotational basis function generally exceeds 0.9, with only a few exceptions when it is 0.8 or greater. It is evident from the above that the quantum dynamics of the rotationally excited CH_4 in the small and large cages is remarkably similar, at least for the low-energy excitations investigated and for the translational ground state of the guest molecule.

The comparison of the rotational energy levels obtained from the purely rotational quantum 3D calculations for the small (Table III) and large cage (Table IV) with their counterparts computed as fully coupled in 6D in Tables V and VI, respectively, shows that they are nearly identical in all aspects. This leads to the conclusion that in both cages the rotations are only weakly coupled to the translational motions, provided that CH_4 is in the translational ground state.

2. Translational excitations

The patterns of the translationally excited 6D T-R energy levels of CH_4 in the small and large cages shown in Tables V and VI, respectively, closely follow the patterns which emerged from the quantum 3D calculations presented in Sec. III A. Consequently, the translational excitations in the small cage are assigned in terms of the quantum numbers n and l of the 3D isotropic HO, while for the translational excitations in

TABLE VI. Select T-R energy levels of CH_4 in the large cavity of sI clathrate hydrate, from the quantum 6D calculations. The T-R excitation energies ΔE are relative to the ground-state energy $E_0=-1313.3$ cm^{-1}. For the purely rotationally excited levels, g denotes their degeneracy. The rms amplitudes Δx, Δy, and Δz are in bohr. The columns labeled $j=0-3$ show the contributions of the corresponding rotational basis functions to the eigenstates. The translational excitations are assigned in terms of the Cartesian quantum numbers (v_x,v_y,v_z) whenever possible, or as $[\mathcal{N}_{xy},v_z]$, where $\mathcal{N}_{xy}$ is the total number of quanta in the x and y modes. For additional explanation see the text.

ΔE	g	Δx	Δy	Δz	$j=0$	$j=1$	$j=2$	$j=3$	
0.0	1	0.36	0.36	0.27	**0.97**	0.00	0.00	0.03	(0,0,0)
9.7	3	0.36	0.36	0.27	0.00	**0.93**	0.06	0.01	(0,0,0)
9.8	3	0.36	0.36	0.27	0.00	**0.93**	0.05	0.01	(0,0,0)
10.3	3	0.36	0.36	0.27	0.00	**0.96**	0.01	0.02	(0,0,0)
25.1	2	0.36	0.36	0.27	0.00	0.00	**0.99**	0.01	(0,0,0)
26.9	2	0.36	0.36	0.27	0.00	0.00	**0.99**	0.01	(0,0,0)
29.1		0.58	0.39	0.26	**0.95**	0.00	0.00	0.05	(1,0,0)
29.5		0.39	0.58	0.26	**0.96**	0.00	0.00	0.04	(0,1,0)
29.5	3	0.36	0.36	0.27	0.00	0.05	**0.91**	0.04	(0,0,0)
30.1	3	0.38	0.36	0.27	0.00	0.09	**0.88**	0.02	(0,0,0)
31.3	3	0.37	0.36	0.27	0.00	0.05	**0.89**	0.05	(0,0,0)
31.7	2	0.36	0.36	0.27	0.00	0.00	**0.99**	0.00	(0,0,0)
31.8	3	0.37	0.37	0.27	0.00	0.09	**0.86**	0.04	(0,0,0)
33.4	3	0.38	0.37	0.27	0.00	0.16	**0.79**	0.04	(0,0,0)
34.4	2	0.36	0.36	0.27	0.00	0.00	**0.98**	0.04	(0,0,0)
41.5	2	0.36	0.36	0.27	0.00	0.00	**0.98**	0.00	(0,0,0)
49.3		0.36	0.36	0.45	**0.91**	0.00	0.00	0.08	(0,0,1)
60.1		0.52	0.51	0.27	**0.62**	0.00	0.00	0.38	[2,0]
60.9		0.58	0.41	0.27	**0.58**	0.00	0.00	0.39	[2,0]
61.3		0.48	0.63	0.26	**0.83**	0.00	0.00	0.16	[2,0]
81.8		0.53	0.44	0.42	**0.85**	0.00	0.00	0.14	(1,0,1)
82.5		0.44	0.54	0.42	**0.88**	0.00	0.00	0.11	(0,1,1)
100.9		0.34	0.34	0.56	**0.78**	0.00	0.00	0.20	(0,0,2)

the large cage the Cartesian quantum numbers (v_x,v_y,v_z) are employed. However, certain quantitative differences are apparent between the energy levels from the quantum 6D calculations and their quantum 3D counterparts. Consider first the *small* cage. For the three components of the translational fundamental $n=1$, $l=1$, the 6D calculations give 73.9, 74.8, and 76.4 cm^{-1} (Table V), while in the 3D calculations they are practically degenerate, 71.5, 71.5, and 71.6 cm^{-1} (Table I). The five $n=2$, $l=2$ states from the 6D calculations range from 147.9 to 150.6 cm^{-1} (Table V), while those from the 3D calculations lie in the slightly narrower interval 143.7–145.5 cm^{-1} (Table I). The same holds for the $n=3$, $l=3$ and $n=3$, $l=1$ multiplets. In general, the 6D results (Table V) show somewhat larger splittings of the n,l multiplets and are shifted by several wave numbers relative to the 3D values (Table I).

For the large cage, comparison of the 6D results (Table VI) with those computed in 3D (Table II) reveals similar trends, although interestingly the differences tend to be smaller than in the case of the small cage. Thus, the fundamental translational excitations in the x, y, and z directions from the 6D calculations are at 29.1, 29.5, and 49.3 cm^{-1}, respectively (their 3D RPDs are shown in Fig. 4), while the 3D calculations give 29.9, 30.0, and 50.5 cm^{-1}. Likewise, for the two-quanta states (1,0,1) and (0,1,1), the 6D results are 81.8 and 82.5 cm^{-1}, respectively, and the 3D values are degenerate, 83.9 cm^{-1}.

We attribute these differences between the energy levels obtained from the 6D calculations and those from the 3D calculations primarily to the T-R coupling, which is rigorously treated in the former and is completely lacking in the latter approach. Additional evidence for the coupling between the translational and rotational degrees of freedom is provided by Tables V and VI, which show significant mixing between the $j=0$ and $j=3$ rotational basis functions in the translationally excited states. Although they are predominantly $j=0$, the $j=3$ contribution can be as high as 40%; an extreme case is the $n=1$, $l=1$ sublevel at 76.4 cm^{-1} in the small cage (Table V), which is 40% $j=0$ and 56% $j=3$. Thus, while for the rotational excitations in the ground translational state the dominant rotational basis function contributes 80% or more (mostly over 90%), translational excitation results in strong $j=0/j=3$ mixing. This makes it difficult to assign with confidence a large fraction of the excited T-R energy levels.

Finally, we point out that our quantum 6D results for the translational fundamentals in the small cage, 73.9–76.4 cm^{-1}, and in the large cage, 29.1–29.5 cm^{-1} in the x/y directions and 49.3 cm^{-1} along the z axis, agree well with the results of the classical MD simulations of sI CH_4 hydrate[24] employing the same CH_4-water interaction potential. Their power spectra associated with the rattling motions of CH_4 have a peak at 70 cm^{-1} attributed to the translational motion of methane molecule in the small cage, and two

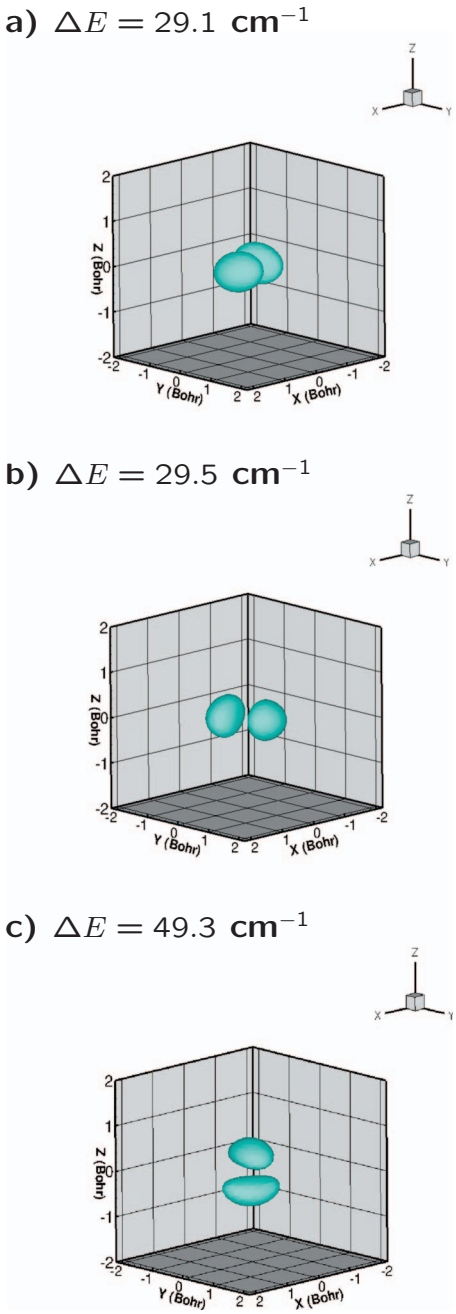

FIG. 4. 3D isosurfaces of the RPD in the Cartesian coordinates of the $j=0$ 6D T-R states of CH_4 in the large cage corresponding to the three translational fundamentals: (a) (1,0,0), (b) (0,1,0), and (c) (0,0,1). The isosurfaces are drawn at 20% of the maximum value of the density. The excitations energies ΔE shown are relative to the ground state, from Table VI.

lower-frequency peaks, at 32 and 52 cm^{-1}, corresponding to the translational motions of methane molecule in the large cage. These classical frequencies, computed for a flexible water framework, differ by only a few wave numbers from the frequencies of the quantum 6D (rigid-cage) translational fundamentals, ~5 cm^{-1} for the small cage and ~3 cm^{-1} for the large cage.

D. Comparison with spectroscopic measurements

The INS spectra of methane hydrate[17,18] taken at $T=5$ K have peaks at 8.7, 17.7, and 26.6 cm^{-1}, which have been assigned to the rotational transitions $j=0\rightarrow1$, $j=1\rightarrow2$, and $j=0\rightarrow2$, respectively, of CH_4. The comparison with our quantum 6D results is not straightforward given the substantial splittings of the computed rotational levels, discussed in Sec. III C. The $j=1$ level is split by 0.4 cm^{-1} in the small cage and by 0.6 cm^{-1} in the large cage, but the splitting of the $j=2$ level is much bigger, 19.7 and 16.4 cm^{-1} in the small and large cages, respectively. Consequently, there is an ambiguity about what energies to use for comparison with the spectroscopic data. If we choose the midpoints of the calculated energy ranges for the $j=1$ and $j=2$ rotational excitations, then our results for the $j=0\rightarrow1$, $j=1\rightarrow2$, and $j=0\rightarrow2$ transitions are 9.8, 22.7, and 32.5 cm^{-1}, respectively, in the small cage, and 10.0, 23.3, and 33.3 cm^{-1}, respectively, in the large cage. Other energies could be chosen for the comparison as well, but irrespective of the details, it is clear that the calculated energies of the three lowest rotational transitions are considerably larger than the experimental values. This signals certain deficiencies of the 6D intermolecular PES used in our calculations, in particular that it overestimates the angular anisotropy of the CH_4-water nanocage interaction. The treatment of the water cages as rigid in our opinion does not likely cause a substantial error in the calculated rotational energy levels.

Despite this quantitative discrepancy, our results are consistent with, and shed light on, several features of the rotational transitions observed in the INS spectra. The calculated energies of the components of the $j=1$ and $j=2$ levels in the small and large cages are very similar, consistent with no evidence for a line splitting of the $j=0\rightarrow1$ transition due to the two different types of cages occupied by the methane molecule.[17,20] The intrinsic linewidth [full width at half maximum (FWHM)] of the $j=0\rightarrow1$ transition at $T=5$ K, 1.6 cm^{-1} (Refs. 17 and 18), has been attributed to the configurational disorder of the H atoms of the framework water molecules, which gives rise to a distribution of the rotational potentials for the methane molecules occupying the cages.[20,18] The calculated splitting of the $j=1$ level due to the angular anisotropy of the PES, 0.4–0.6 cm^{-1}, contributes little to the observed linewidth, especially since the true anisotropy-induced $j=1$ splitting is likely to be considerably smaller. However, the $j=0\rightarrow2$ transition is much broader,[17] with the measured linewidth (FWHM) of 6.5 cm^{-1}. Its greater width can be understood to arise from the multitude of rotational transitions from the $j=0$ state to the ten components of the $j=2$ level which are substantially spread, over 19.7 and 16.4 cm^{-1} in the small and large cages, respectively. These closely spaced transitions cannot be resolved in the INS spectra due to instrumental limitations and appear as a broadening of the observed rotational excitations.

Comparison of our calculated translational excitations of the caged CH_4 with the INS spectroscopic data is more complicated due to the difficulties with the interpretation of the experimental results, which were outlined in the Introduction. Three excitations, with the maxima at 43.6, 61.3, and 80.7 cm^{-1}, were identified in the INS spectra of methane in the host clathrate, which was deuterated in order to diminish the contributions of the host vibrations to the spectrum.[21] The two-lower frequency peaks were attributed to the translational excitations of CH_4 in the large cage, in the directions

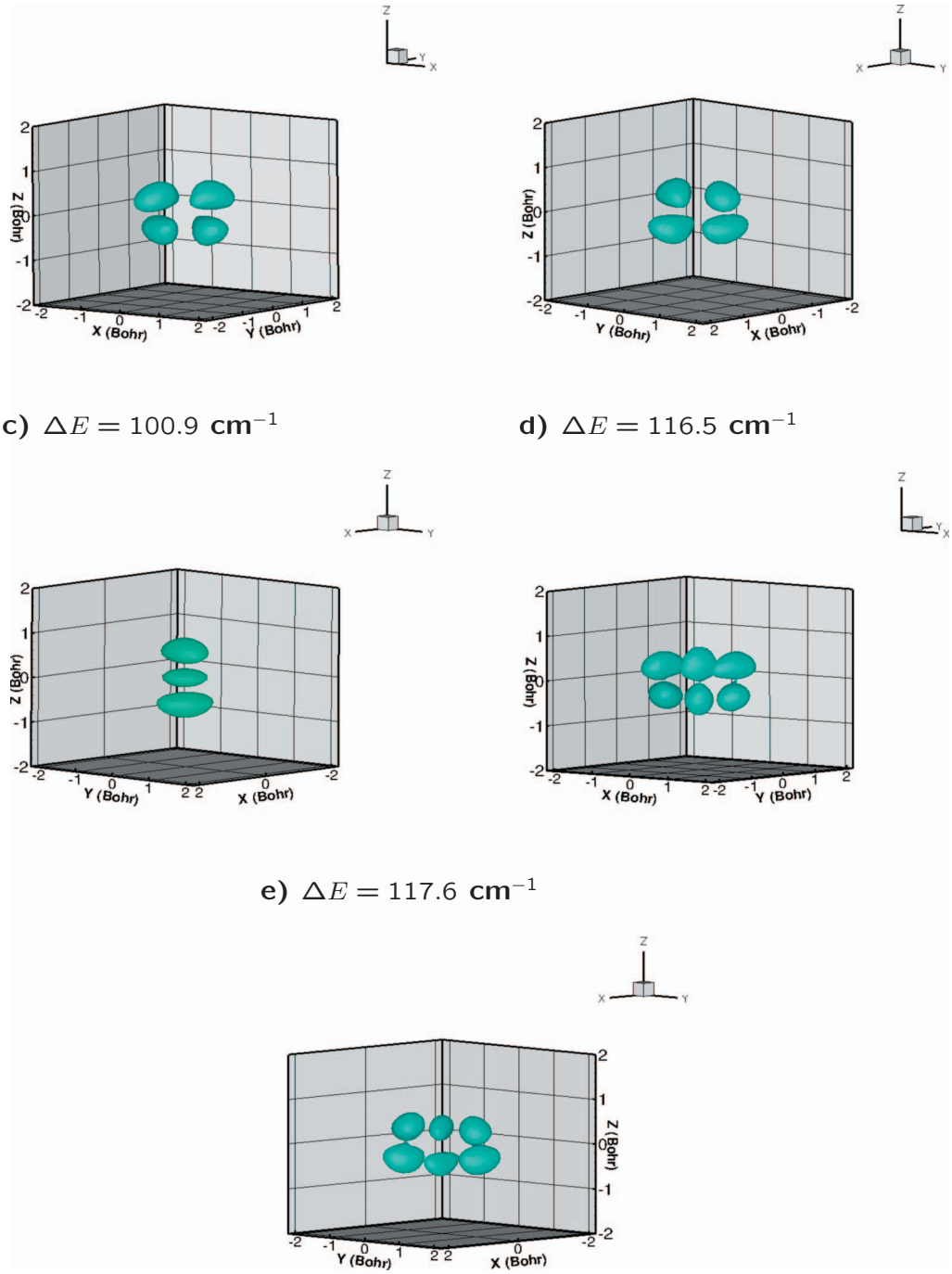

FIG. 5. 3D isosurfaces of the RPD in the Cartesian coordinates of several $j=0$ 6D T-R states of CH_4 in the large cage, with two or more quanta of excitation: (a) (1,0,1), (b) (0,1,1), (c) (0,0,2), (d) (2,0,1), and (e) (0,2,1). The isosurfaces are drawn at 20% of the maximum value of the density. The excitations energies ΔE shown are relative to the ground state.

of its long and short axes, respectively, and the highest-frequency peak was tentatively associated with the CH_4 translational fundamental in the small cage.[21] Our calculated frequencies of the translational fundamentals are 29.1, 29.5, and 49.3 cm^{-1} in the large cage, and 73.9, 74.8, and 76.4 cm^{-1} in the small cage (the $n=1$, $l=1$ triplet). They are considerably lower than corresponding measured frequencies, which would suggest that the PES employed is too soft, and the CH_4-water interaction insufficiently repulsive. However, the host lattice modes are known to have maxima which overlap in part with the two higher-energy experimental peaks above,[21,22] and there is some evidence of coupling between the guest and host lattice vibrations as well. This leaves the peak measured at 43.6 cm^{-1} as the only one which can be confidently assigned to the CH_4 translational excitation (in the large cage), largely free from the contributions of the water framework vibrations. But, in our opinion, the guest-host coupling is unlikely to result in large shifts of the translational frequencies of the encapsulated methane. This is supported by the good agreement noted in Sec. III C

between the frequencies of the translational fundamentals for methane in the small and large cages from our quantum 6D calculations and those obtained from the classical MD simulations; the latter are performed for a flexible host lattice and include at least approximately the coupling between its vibrations and the T-R modes of methane. Therefore, we believe that the differences between the calculated translational excitations of CH_4 and those measured by the INS spectra are indicative of the shortcomings of the 6D PES and can be used to guide its improvement.

IV. CONCLUSIONS

We reported the results of the first rigorous quantum dynamics study of the 6D T-R eigenstates of methane molecule in the small and large cages of the sI clathrate hydrate. This study had two main goals. One was to develop the computational methodology for the efficient and accurate quantum 6D calculations of the T-R energy levels and wave functions of a polyatomic molecule confined inside a nanocavity. In our approach, both the guest molecule and the cavity are assumed to be rigid, while the three translational and three rotational degrees of freedom of the guest molecule are treated as fully coupled. Our computational procedure involves solving two reduced-dimension (3D) eigenvalue problems for the translational and rotational motions, respectively. Truncated sets of their 3D eigenvectors serve as the contracted translational and angular basis functions. The matrix of the full 6D T-R Hamiltonian in this compact product contracted 6D basis is diagonalized, yielding the T-R energy levels and wave functions, which are numerically exact for the 6D intermolecular PES employed. In the present study, this scheme was implemented for a spherical top (CH_4), but it can be readily extended and applied to nanoconfined rotors of lower symmetry, symmetric and asymmetric tops (e.g., H_2O).

The second objective of this study was to provide a quantitative description of the quantum dynamics of the coupled translational and rotational motions of the caged CH_4 molecule. A pairwise additive CH_4-nanocage PES was used, based on the anisotropic CH_4—H_2O pair potential of Tse *et al.*,[24] which they and others[16,26,30] utilized in the classical MD simulations of CH_4 hydrate. Our calculations revealed that the $(2j+1)^2$ degeneracy of the rotational levels of CH_4 in the gas phase with the quantum number j is partially lifted by the angular anisotropy of the PES, resulting in rather intricate patterns of splittings of the rotational multiplets. In the small and large cages, the rotational levels corresponding to $j=1$, 2, and 3, are split into 3, 10, and 21 components, respectively, many of which are doubly or triply degenerate. For the rotational excitations considered, j is a good quantum number since the contribution of the dominant rotational basis function is generally greater than 0.9. Not only are the splitting patterns identical in both types of cages for a given j value, but the actual energies of the rotational sublevels are very similar as well, evidence that for the low-lying rotational eigenstates the quantum dynamics of CH_4 is virtually the same in the small and large cages, provided that the molecule is ground translational state.

Inspection of the T-R energy level patterns, rms amplitudes, and the 3D RPDs in the Cartesian coordinates of the 6D T-R wave functions showed that the translational excitations of CH_4 in the small cage can be assigned in terms of the quantum numbers n and l of the 3D isotropic HO. On the other hand, for the translationally excited 6D T-R levels in the large cage, the Cartesian quantum numbers (v_x,v_y,v_z) proved to be more appropriate. These two distinct sets of translational quantum numbers correlate well with the symmetries of the two cages, spherical top for the small cage and (oblate) symmetric top for the large cage, when only the O atoms of the water molecules are taken into account. The coupling between the translational and rotational degrees of freedom of CH_4 is evident from the strong mixing of the (dominant) $j=0$ and $j=3$ rotational basis functions in the translationally excited T-R eigenstates.

Our quantum 6D results for the $j=0\rightarrow1$, $j=1\rightarrow2$, and $j=0\rightarrow2$ rotational transitions, 10, 23, and 33 cm^{-1}, respectively, are larger than the corresponding INS spectroscopic values, 9, 18, and 27 cm^{-1}, respectively.[17,18] This implies that the 6D PES employed exaggerates the actual angular anisotropy of the methane-water nanocage interaction. The frequencies of translational fundamentals from our quantum 6D calculations, 29 and 49 cm^{-1} in the large cage and $\sim$75 cm^{-1} in the small cage, are appreciably lower than those extracted from the INS spectra of methane hydrate,[21] 44, 61, and 81 cm^{-1}. The comparison of the calculated and measured translational fundamentals has some ambiguities, due to the considerable overlap between the frequencies of the translations of CH_4 and those of the water framework vibrations, and the coupling of the guest and host lattice modes whose strength is not known accurately. Nevertheless, we believe that the discrepancies between the calculated and experimental translational excitations are caused primarily by the deficiencies of the 6D PES, and can therefore provide guidance for its refinement.

These quantitative differences notwithstanding our results are consistent with and illuminate a number of salient features of the INS spectroscopic data for methane hydrate. Our future work will involve more sophisticated methane-cage interaction potentials, as well as extensions to the calculation of the transition probabilities and hence the intensities of the bands observed in the INS spectra.

ACKNOWLEDGMENTS

I.M. is grateful to the Unity through Knowledge Fund of Croatia for funding this research through Gaining experience Grant No. 12. Z.B. is grateful to the National Science Foundation for partial support of this research through Grant No. CHE- 0315508. The computational resources used in this work were funded in part by the NSF MRI Grant No. CHE-0420870. Acknowledgment is made to the donors of the American Chemical Society Petroleum Research Fund for partial support of this research.

[1] W. L. Mao, C. A. Koh, and E. D. Sloan, Phys. Today **60**, 42 (2007).
[2] V. V. Struzhkin, B. Militzer, W. L. Mao, H. K. Mao, and R. J. Hemley, Chem. Rev. (Washington, D.C.) **107**, 4133 (2007).
[3] E. D. Sloan, *Clathrate Hydrates of Natural Gases* (Marcel Dekker, New

York, 1998).
[4] E. D. Sloan, Jr., Nature (London) **426**, 353 (2003).
[5] B. A. Buffett, Annu. Rev. Earth Planet. Sci. **28**, 477 (2000).
[6] C. Gutt, B. Asmussen, W. Press, M. R. Johnson, Y. P. Handa, and J. S. Tse, J. Chem. Phys. **113**, 4713 (2000).
[7] A. Hoshikawa, N. Igawa, H. Yamauchi, and Y. Ishii, J. Chem. Phys. **125**, 034505 (2006).
[8] M. Xu, Y. Elmatad, F. Sebastianelli, J. W. Moskowitz, and Z. B. Bačić, J. Phys. Chem. B **110**, 24806 (2006).
[9] M. Xu, F. Sebastianelli, and Z. B. Bačić, J. Chem. Phys. **128**, 244715 (2008).
[10] F. Sebastianelli, M. Xu, and Z. B. Bačić, J. Chem. Phys. **129**, 244706 (2008).
[11] M. Xu, F. Sebastianelli, and Z. B. Bačić, J. Phys. Chem. A **113**, 7601 (2009).
[12] M. Xu, F. Sebastianelli, Z. B. Bačić, R. Lawler, and N. J. Turro, J. Chem. Phys. **128**, 011101 (2008).
[13] M. Xu, F. Sebastianelli, Z. B. Bačić, R. Lawler, and N. J. Turro, J. Chem. Phys. **129**, 064313 (2008).
[14] M. Xu, F. Sebastianelli, B. R. Gibbons, Z. B. Bačić, R. Lawler, and N. J. Turro, J. Chem. Phys. **130**, 224306 (2009).
[15] G. Tarrago, M. Dang-Nhu, G. Poussigue, G. Guelachvili, and C. Amiot, J. Mol. Spectrosc. **57**, 246 (1975).
[16] J. S. Tse, C. I. Ratcliffe, B. M. Powell, V. F. Sears, and Y. P. Handa, J. Phys. Chem. A **101**, 4491 (1997).
[17] C. Gutt, B. Asmussen, W. Press, C. Merkl, H. Casalta, J. Greinert, G. Bohrmann, J. S. Tse, and A. Hüller, Europhys. Lett. **48**, 269 (1999).
[18] C. Gutt, W. Press, A. Hüller, and J. S. Tse, Appl. Phys. A: Mater. Sci. Process. **74**, s1299 (2002).
[19] M. Prager and W. Press, J. Chem. Phys. **125**, 214703 (2006).
[20] C. Gutt, W. Press, A. H. Uller, J. S. Tse, and H. Casalta, J. Chem. Phys. **114**, 4160 (2001).
[21] J. Baumert, "Structure, lattice dynamics, and guest vibrations of methane and xenon hydrate," Ph.D. thesis, Christian-Albrechts University, Kiel, Germany, 2003.
[22] J. Baumert, C. Gutt, V. P. Shpakov, J. S. Tse, M. Krisch, M. Müller, H. Requardt, D. D. Klug, S. Janssen, and W. Press, Phys. Rev. B **68**, 174301 (2003).
[23] J. S. Tse, M. L. Klein, and I. R. McDonald, J. Phys. Chem. **87**, 4198 (1983).
[24] J. S. Tse, M. L. Klein, and I. R. McDonald, J. Chem. Phys. **81**, 6146 (1984).
[25] H. Tanaka and K. Kiyohara, J. Chem. Phys. **98**, 8110 (1993).
[26] N. J. English and J. M. D. Macelroy, J. Comput. Chem. **24**, 1569 (2003).
[27] J. A. Greathouse, R. T. Cygan, and B. A. Simmons, J. Phys. Chem. B **110**, 6428 (2006).
[28] H. Jiang, K. D. Jordan, and C. E. Taylor, J. Phys. Chem. B **111**, 6486 (2007).
[29] H. Jiang, E. M. Myshakin, K. D. Jordan, and R. P. Warzinski, J. Phys. Chem. B **112**, 10207 (2008).
[30] S. Alavi, J. A. Ripmeester, and D. D. Klug, J. Chem. Phys. **126**, 124708 (2007).
[31] N. J. English and J. S. Tse, Phys. Rev. Lett. **103**, 015901 (2009).
[32] J. S. Tse, V. P. Shpakov, V. V. Murashov, and V. R. Belosludov, J. Chem. Phys. **107**, 9271 (1997).
[33] S. Liu, Z. Bačić, J. W. Moskowitz, and K. E. Schmidt, J. Chem. Phys. **103**, 1829 (1995).
[34] J. Echave and D. C. Clary, Chem. Phys. Lett. **190**, 225 (1992).
[35] H. Wei and T. Carrington, Jr., J. Chem. Phys. **97**, 3029 (1992).
[36] Z. Bačić and J. C. Light, Annu. Rev. Phys. Chem. **40**, 469 (1989).
[37] M. E. Rose, *Elementary Theory of Angular Momentum* (Wiley, New York, 1957).
[38] R. N. Zare, *Angular Momentum: Understanding Spatial Aspects in Chemistry and Physics* (Wiley-Intersience, New York, 1988).
[39] J. M. Bowman, T. Carrington, and H. D. Meyer, Mol. Phys. **106**, 2145 (2008).
[40] S. McDonald, L. Ojamäe, and S. J. Singer, J. Phys. Chem. A **102**, 2824 (1998).
[41] H. J. C. Berendsen, J. R. Grigera, and T. P. Straatsma, J. Phys. Chem. **91**, 6269 (1987).
[42] L. D. Landau and E. M. Lifshitz, *Quantum Mechanics* (Pergamon, Oxford, 1977).
[43] L. Ulivi, M. Celli, A. Gianassi, A. J. Ramirez-Cuesta, D. J. Bull, and M. Zoppi, Phys. Rev. B **76**, 161401 (2007).
[44] A. Giannasi, M. Celli, L. Ulivi, and M. Zoppi, J. Chem. Phys. **129**, 084705 (2008).
[45] T. A. Strobel, E. D. Sloan, and C. A. Koh, J. Chem. Phys. **130**, 014506 (2009).
[46] R. E. Miller and J. C. Decius, J. Chem. Phys. **59**, 4871 (1973).
[47] T. Momose, J. Chem. Phys. **107**, 7695 (1997).
[48] T. Momose, H. Hoshina, M. Fushitani, and H. Katsuki, Vib. Spectrosc. **34**, 95 (2004).